oxygen

MDPI

Article

Characterization of Mixed Metal Biogenic Manganese Oxide Materials for Catalysis and Rare Earth Element Sequestration

Elisa Morales [1], Jeremy Brown [2], Chloe Runge [2], Madeline York [2], Genesis Dennis [1], Cole Johnson [1], Anthony Baudino [1], Norman Paz-Ramirez [1], Lily Samson [2], John Rey A. Romal [3], Kari L. Stone [1,*] and Sarah E. Shaner [2,*]

[1] Department of Chemistry, Lewis University, One University Pkwy, Romeoville, IL 60446, USA; elisamorales@lewisu.edu (E.M.); genesisdennis@lewisu.edu (G.D.); coledjohnson@lewisu.edu (C.J.); anthonymbaudino@lewisu.edu (A.B.); normanapazramirez@lewisu.edu (N.P.-R.)
[2] Department of Chemistry and Physics, Southeast Missouri State University, Cape Girardeau, MO 63701, USA; jobrown3s@semo.edu (J.B.); crunge1s@semo.edu (C.R.); mpyork1s@semo.edu (M.Y.); lilsamson03@gmail.com (L.S.)
[3] Department of Civil and Environmental Engineering, University of Wisconsin-Platteville, 1 University Plaza, Platteville, WI 53818, USA; romalj@uwplatt.edu
* Correspondence: kstone1@lewisu.edu (K.L.S.); sshaner@semo.edu (S.E.S.)

Abstract

This study explores the potential of utilizing biogenic manganese oxides (BMOs) produced by Mn-oxidizing *Pseudomonas putida* MnB1 to facilitate metal cation uptake for rare earth element (REE) sequestration and the synthesis of novel materials. Previous studies have shown that *P. putida* MnB1 efficiently oxidizes environmental Mn(II) to Mn(IV)-oxides, producing BMOs with unique physicochemical properties. Unlike their abiotic counterparts, BMOs exhibit high surface area, reactivity, and amorphous, poorly crystalline structures, making them promising platforms for adsorbing metal cations. This research study, building on the prior work, demonstrates the incorporation of ten different main group, transition, and rare earth metals into the BMO material, with structural characterization conducted via scanning electron microscopy and powder X-ray diffraction. Compositional characterization was determined by inductively coupled plasma optical emission spectroscopy and energy dispersive X-ray spectroscopy via scanning electron microscopy. Following the initial screening of these ten cations, batch adsorption studies were performed for a representative light REE, heavy REE, and transition metal-spiked sample prepared with real wastewater effluent indicating that the BMO material in this study is promising for sequestering REEs from real water streams. These findings advance the understanding of biologically mediated metal adsorption and open pathways for designing new functional materials with potential applications in rare earth sequestration and catalysis. To highlight this later point, the BMO materials with an incorporated main group (Al^{3+}, Ca^{2+}) or transition metal cation (Fe^{3+}, Cu^{2+}) were tested electrochemically for their ability to act as water oxidation catalysts, and each of these materials' activity was comparable to BMO except for the material with incorporated iron, which showed significantly enhanced activity.

Keywords: biogenic manganese oxide; metal oxide; MnO_x; Mn-oxidizing bacteria; MnB1; rare earth elements; critical element sequestration; wastewater effluent; water oxidation; oxygen evolution; catalysis

Check for updates

Academic Editor: John T. Hancock

Received: 19 March 2026
Revised: 6 May 2026
Accepted: 15 May 2026
Published: 20 May 2026

Copyright: © 2026 by the authors. Licensee MDPI, Basel, Switzerland. This article is an open access article distributed under the terms and conditions of the Creative Commons Attribution (CC BY) license.

1. Introduction

Manganese oxides (MnO_x) are versatile materials recognized for their roles in catalysis and environmental remediation of metal and organic pollutants. Their catalytic activity in redox chemistry [1,2], the oxygen evolution reaction (OER) [3–7], and organic pollutant degradation [8–12] arises from multiple Mn oxidation states (Mn^{2+}, Mn^{3+}, Mn^{4+}), structural polymorphism, and redox-active surfaces [13]. Additionally, MnO_x materials serve as effective adsorbents for metal cations, including rare earth elements (REEs) [14] and heavy metals [15–19]. While abiotic manganese oxides may be synthesized via several routes including hydrothermal, colloidal, and electrochemical methods, which allow for precise control over phase, morphology, and composition through doping and nanostructuring [20–22], biogenic manganese oxides (BMOs) are formed by Mn(II)-oxidizing fungi or bacteria such as *Pseudomonas putida* MnB1 and *Bacillus* sp. under ambient conditions. These BMOs typically exhibit layered MnO_2 structures with poor crystallinity, high surface areas, and enhanced reactivity. For example, they have been shown to oxidize contaminants like diclofenac at rates significantly higher than their synthetic analogs [9], and due to the presence of vacancies and/or Mn(III) sites, BMOs facilitate adsorption of metal cations with a wide range of charges, sizes, and bonding geometries [23–26].

This study investigates the propensity for biogenic manganese oxides produced by the organism *Pseudomonas putida* MnB1 to adsorb a wide range of metal cations including critical metals such as rare earth elements. This study screens for the adsorption of ten different metal cations and, using inductively coupled plasma optical emission spectroscopy (ICP-OES), scanning electron microscopy with energy-dispersive X-ray spectroscopy (SEM-EDX), and X-ray diffraction (XRD), confirms successful metal integration, stable morphology, and retention of disordered structures upon metal uptake by our BMO material. This initial screening for adsorption of main group, transition, and rare earth metal cations suggests that this is a possible approach for metal sequestration and also provides a straightforward route to prepare mixed metal BMO materials. The ability for the BMO material to perform metal adsorption under real world conditions was probed through batch adsorption studies using representative light REE (Nd^{3+}), heavy REE (Dy^{3+}), and transition metal (Cu^{2+}) cations in real wastewater effluent and indicates that the material is promising for sequestering REEs from real water streams. Finally, to explore one application related to renewable energy, four of the mixed metal BMO materials produced via the metal uptake studies were tested for their ability to serve as water oxidation catalysts. In these electrochemical studies, three of the mixed metal BMO materials showed activity similar to BMO. However, the material that had adsorbed iron showed significantly improved OER activity. This work establishes a scalable, green approach that merges the advantages of biogenic manganese oxide with the functional benefits of metal doping, yielding sustainable materials for potential energy and environmental applications.

2. Materials and Methods

2.1. MnO_x Material Preparation

2.1.1. Preparation of Whole-Cell BMO

Cultures of 10 mL of *Pseudomonas putida* (Trevisan) Migula MnB1 supplied by American Type Culture Collection (ATCC #23483) (Manassas, VA, USA) were prepared and grown at room temperature or 30 °C for 3 days. Liquid growth media (250 mL) was prepared according to Jiang et al. [27]. The Liquid growth medium's composition was 0.5 g/L yeast extract, 0.5 g/L casamino acid, 1 g/L glucose, 2.38 g/L HEPES buffer, 0.222 g/L $CaCl_2$, 0.8118 g/L $MgSO_4{\cdot}7H_2O$, 0.001 g/L $FeCl_3{\cdot}6H_2O$, 0.1145 g/L $MnCl_2$, and 1 mL/L trace element solution. The trace element solution composition was 6.4 mg/L $CuSO_4$, 44 mg/L $ZnSO_4{\cdot}7H_2O$, 20 mg/L $CoCl_2{\cdot}6H_2O$ and 13 mg/L $Na_2MoO_4{\cdot}2H_2O$.

Cultures were added to the liquid growth media and incubated at 24 °C while shaking for four days. Dark-brown or black precipitates formed, indicating the formation of BMOs. Cell material containing the BMO was collected through centrifugation at 3000 rpm for 10 min. Roughly 80–100 mg of cell material was produced. Supernatant was removed as much as possible and the remaining solid was stored.

2.1.2. Synthesis of Birnessite

Birnessite was prepared as a synthetic reference material for comparison to biogenic manganese oxide. The synthesis was carried out according to the procedure used by Tao and Britt and described by Villalobos et al. [3,24]. Briefly, an aqueous solution of $MnCl_2 \cdot 4H_2O$ (Spectrum Chemical, Gardena, CA, USA, 3.166 g dissolved in 32 mL of water) was added dropwise to an aqueous solution of NaOH (Flinn Scientific, Batavia, IL, USA, 11.0321 g in 36 mL of water) and stirred vigorously to produce a peach/pink precipitate. Next, an aqueous solution of $KMnO_4$ (Fisher Chemicals, Fair Lawn, NJ, USA, 1.0035 g in 32 mL of water) was added dropwise to the mixture. The mixture was stirred for 1 h and a dark gray/brown solid formed. The mixture was covered in foil and stirred at 55 °C for 24 h. The supernatant was decanted and discarded, and the remaining mixture was centrifuged. The solid was washed five times with a 1 M NaCl solution followed by washing 10 times with distilled water. The birnessite was dried via lyophilization and stored in the dark.

2.2. Metal Uptake Studies

The ability of BMO samples to adsorb the metal cations Al^{3+}, Ca^{2+}, Fe^{3+}, Cu^{2+}, La^{3+}, Ce^{3+}, Pr^{3+}, Nd^{3+}, Eu^{3+}, and Dy^{3+} was investigated through a series of metal uptake studies. Metal salts were obtained from commercial sources and used without further purification. The compounds used were $Al_2(SO_4)_3 \cdot 16H_2O$, $CaCl_2$, $(NH_4)_2Fe(SO_4)_2 \cdot 6H_2O$, $CuSO_4 \cdot 5H_2O$, $La(NO_3)_3 \cdot 6H_2O$, $Ce(NO_3)_3 \cdot 6H_2O$, $Pr(NO_3)_3 \cdot 6H_2O$, $Nd(NO_3)_3 \cdot 6H_2O$, $EuCl_3 \cdot 6H_2O$, and $Dy(NO_3)_3 \cdot 6H_2O$. The BMO material used was the whole cell material, described in Section 2.1.1, containing MnO_x and cellular material. To test each metal, a 100 ppm solution of each was prepared in DI water, and 10 mL of this solution was added to the BMO material (~80 mg). This mixture was vigorously shaken for 5–10 min before centrifuging at 3000 rpm for 10 min. The metal solution was carefully decanted without disturbing the BMO pellet, and the resulting material was vacuum dried. This procedure was followed to test each of the 10 metal cations independently, and an additional two competition-type studies were also performed. A metal uptake study with a 100 ppm metal solution of 1:1 cerium and europium was carried out, as was an analogous study with 1:1 lanthanum and dysprosium.

2.3. Powder X-Ray Diffraction

Powder X-ray diffraction (XRD) data on birnessite, BMO, and BMO samples after metal uptake experiments were collected at room temperature with a Rigaku SmartLab SE diffractometer (Rigaku Corporation, Tokyo, Japan) using a copper anode (with Kα1 = 1.54056 Å and Kα2 = 1.54439 Å) fitted with a nickel Kβ filter. Samples were placed on a zero-background sample holder and analyzed between a 2θ range of 5 and 80° with a step size of 0.01 degrees and scan speed of 1 degree/min.

2.4. Scanning Electron Microscopy

Scanning electron microscope (SEM) images with complementary energy-dispersive X-ray (EDX) spectroscopy data were collected using a JEOL JCM 7000 scanning electron microscope (JEOL Ltd., Tokyo, Japan). Samples for analysis were deposited onto carbon tape and secured on an atomically flat silica wafer, that was precoated using 10 nm Au

nanoparticles to reduce charging. EDX was used to quantify and map relevant elements. For all samples, manganese, calcium, and potassium were measured. For M BMO samples, the metal used in the uptake study was also measured, and a BMO control sample was also tested for Mn, Ca, K, and that metal at the same time. For example, for the La BMO sample, SEM-EDX was used to measure the relative amounts of Mn, Ca, K, and La in the material, and a BMO sample was also tested for Mn, Ca, K, and La at the same time.

2.5. Determination of Metal Content via ICP-OES

Inductively coupled plasma optical emission spectroscopy was performed with a Perkin Elmer Optima 8000 instrument (PerkinElmer, Inc., Shelton, CT, USA). To prepare the samples, around 10 mg of BMO material was dissolved in 1 mL of concentrated nitric acid for 18–24 h, and resulting solutions were diluted to 10.0 mL in volumetric flasks. When necessary, these solutions were then subjected to further 10-fold or 100-fold dilutions. All samples were analyzed for Mg, Al, K, Ca, Mn, Fe, and Cu. Calibration standards with concentrations between 1 ppm and 100 ppm were prepared by diluting a 100 ppm multi-element standard (Instrument Calibration Standard 2, SPEX CertiPrep, Metuchen, NJ, USA). Samples expected to contain rare earth elements were also analyzed for La, Ce, Pr, Nd, Eu, and Dy, and calibration standards with concentrations between 1 and 50 ppm were prepared by diluting a 50 ppm rare earth multi-element standard (rare earth element mix for ICP, Sigma Aldrich, Buchs, Switzerland).

2.6. Batch Adsorption Studies and Adsorption Isotherms

A series of batch adsorption studies was conducted to obtain adsorption isotherms for three representative metal types: light rare earth elements, heavy rare earth elements, and transition metals, namely, Nd^{3+}, Dy^{3+}, and Cu^{2+}, respectively, in real water streams to demonstrate practical compatibility of BMO for REE sequestration. The wastewater sample matrix used in this study was collected by a grab-sample method from the treated discharge of a municipal wastewater treatment facility in Southern Wisconsin, serving a residential population of ~12,000 and an additional post-secondary student population of ~6500. The effluent collected had a pH of 7.4 $\pm$ 4 and a conductivity of 1600 µS/cm. The treated wastewater contained Ca, Mg, K, and Na at 44, 15, 4, and 65 mg/L, respectively, and traces of transition metals including Cu, Fe, Mn, and Zn at 110, 90, 2, and 1.4 µg/mL, respectively, whereas the nitrate concentrations can vary depending on the time of the day and days of the week the discharge is collected. To test the adsorption capacity of BMO for REEs and transition metals from real and complex water matrices, the treated wastewater sample was dosed with 15 mg/L of Nd^{3+}, Dy^{3+}, and Cu^{2+} to represent transition metals. The pH was adjusted to a pH of 4.5 $\pm$ 2 to ensure solubility of metals, resulting in a conductivity of 2500 µS/cm. These metal concentrations are typically observed in industrial wastewater streams.

The batch adsorption studies were performed by dosing 10 mL of Cu^{2+}/Nd^{3+}/Dy^{3+}-spiked wastewater with powderized BMO at a dosage of 0.5, 1.1, 2.1, 5.2, 10, and 14.9 g/L. The suspension was agitated on a platform shaker at 25 °C for 20 min. The suspension was allowed to settle and the resulting supernatant was filtered with a 0.45 µm filter, then analyzed for metal content by ICP-OES. The isotherms for Nd^{3+}, Dy^{3+}, and Cu^{2+} were generated using the same data set, fitting the experimental data from the batch adsorption experiments into the non-linearized Langmuir and Freundlich isotherm described in Equations (1) and (2), respectively, in OriginPro 2026 v10.3 software (OriginLab Corporation, Northampton, MA, USA) to obtain the maximum adsorption capacity of these metals onto BMO in real wastewater.

$$q_e = \frac{q_m K_L C_e}{1 + K_L C_e} \quad (1)$$

$$q_e = K_F C_e^{\frac{1}{b}} \quad (2)$$

In these equations, q_e is the equilibrium adsorption capacity (mg/g), C_e is the equilibrium concentration (mg/L), q_m is the maximum adsorption capacity (mg/g), K_L is the Langmuir constant, K_F is the Freundlich constant, and b is the exponential constant to the Freundlich equation.

2.7. Electrochemical Water Oxidation

Electrochemical water oxidation experiments were modified from the procedure described by Stahl et al. [6]. Catalyst inks were prepared by combining 5 mg of catalyst (BMO or M BMO), 5 mg of carbon black acetylene (Thermo Scientific Chemicals, Ward Hill, MA, USA), 45 µL of 5% wt% Nafion (Thermo Scientific Chemicals, Ward Hill, MA, USA), and 350 µL of ethanol. The ink was sonicated for 10 min. Glassy carbon electrodes (3 mm, BASi, West Lafayette, IN, USA) were polished with an alumina slurry on a felt pad and rinsed with water and ethanol prior to the deposition of 5 µL of the catalyst ink. The electrode was dried at room temperature for 10 min followed by 70 °C for 10 min. The electrodes were allowed to cool to room temperature and were wetted with a few drops of water before electrochemical analysis.

Electrochemical experiments were performed with a CH Instruments 620E Electrochemical Analyzer (CH Instruments, Inc., Austin, TX, USA) using a standard three-electrode cell. A Ag/AgCl reference electrode and platinum wire counter electrode were used in addition to the glassy carbon working electrode with the ink. Linear sweep voltammetry (LSV) was performed in a stirred aqueous 0.1 M NaOH solution at a scan rate of 5 mV/s. Scans were performed by scanning from 0 mV to 1200 mV vs. Ag/AgCl. For each electrode, two LSV scans were performed, and in all cases, data from the second scan were used. Reported LSV data are the average of three electrodes.

3. Results

The biogenic manganese oxide material used in this study was produced by the organism *Pseudomonas putida* MnB1. As previously described, cultures of the bacteria were incubated with a liquid growth media containing Mn(II). After four days, dark brown or black precipitate was visible, and the solid containing the BMO and cell material was isolated, washed, and dried under vacuum [5]. This whole-cell BMO material containing MnO_x and cellular material was used without further purification or workup and is referred to as BMO. The ability of BMO samples to adsorb main group (Al^{3+}, Ca^{2+}), transition (Fe^{3+}, Cu^{2+}), and rare earth (La^{3+}, Ce^{3+}, Pr^{3+}, Nd^{3+}, Eu^{3+}, Dy^{3+}) metals was investigated through a series of metal uptake screening studies in which BMO material was vigorously shaken with a 100 ppm metal solution for 5–10 min. Each of the 10 metal cations were tested independently, but two competition-type studies were also performed. A metal uptake study with a 100 ppm metal solution of 1:1 cerium and europium was carried out, as was an analogous study with 1:1 lanthanum and dysprosium. For all studies, following exposure to the 100 ppm metal cation solution, BMO material was isolated by centrifugation and characterized by powder X-ray diffraction, ICP-OES, and SEM-EDX to determine the effect on BMO's structure and composition. Following the uptake studies, the resulting materials are referred to as M BMO, where M is the chemical symbol for the metal used in the uptake experiment.

The structures of the M BMO materials following the metal uptake studies were investigated by powder X-ray diffraction and compared to the structures of synthetic birnessite and BMO that had not been subjected to additional metals. The diffraction patterns of the BMOs exposed to main group and transition metal cations are shown in Figure 1 and those exposed to rare earth cations are shown in Figure 2. The synthetic

birnessite pattern shows peaks consistent with a crystalline layered δ-MnO_2 structure, while the pattern from the BMO sample shows no well-defined peaks and is consistent with an amorphous material, which has been widely reported for biogenic manganese oxides [23]. Following the metal uptake experiments, all of the diffraction patterns from the resulting M BMO materials are unchanged, indicating that the structure of BMO remains amorphous and is not affected by exposure to the metal solutions in a way that is detectable by XRD.

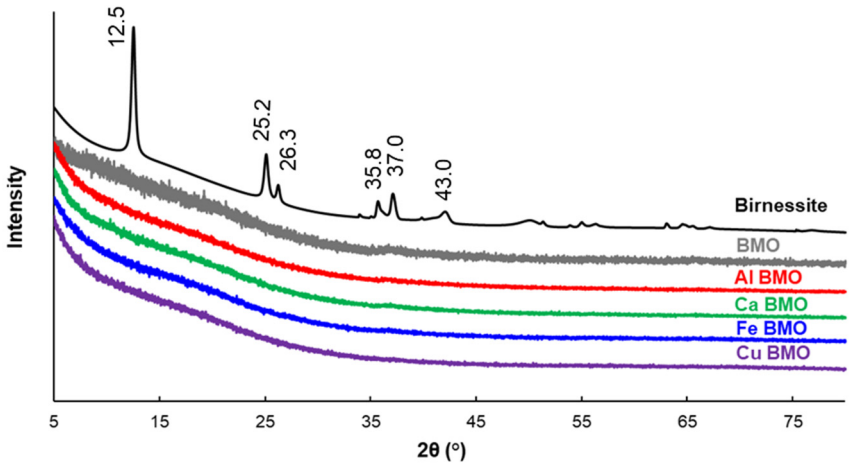


Figure 1. Powder X-ray diffraction patterns of birnessite, BMO, and M BMO materials following metal uptake studies with a 100 ppm main group or transition metal cation solution.

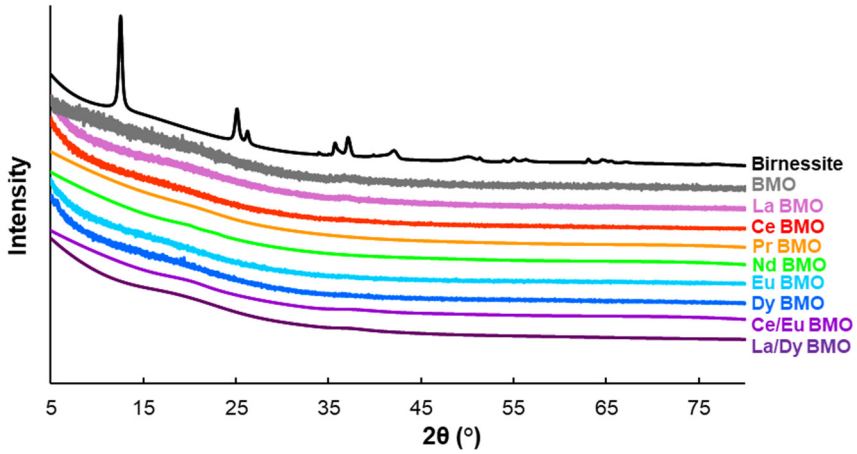


Figure 2. Powder X-ray diffraction patterns of birnessite, BMO, and M BMO materials following metal uptake studies with a 100 ppm rare earth metal cation solution. For the Ce/Eu BMO and La/Dy BMOs, the solutions used were a 1:1 mixture of the two metal cations.

Images of the BMO material and the BMO samples after the metal uptake studies were obtained with a scanning electron microscope and are shown in Figure S1, Figures 3 and 4 for the BMO, main group and transition metal M BMO, and rare earth M BMO, respectively. The resulting SEM images show amorphous materials. The EDX element maps of BMO and M BMO samples indicate that manganese is present and evenly distributed throughout all of the samples, and for the M BMO samples, the second metal is also present uniformly throughout the image. The possible exceptions are Ce BMO and Ce/Eu BMO where the cerium appears to be more concentrated along the edges of the features. For comparison, the SEM images of MnB1 cellular material grown in the absence of manganese before and after a metal uptake study performed with a 100 ppm iron solution are shown in Figure S2, and images of birnessite following a metal uptake study performed with 100 ppm iron are shown in Figure S3.

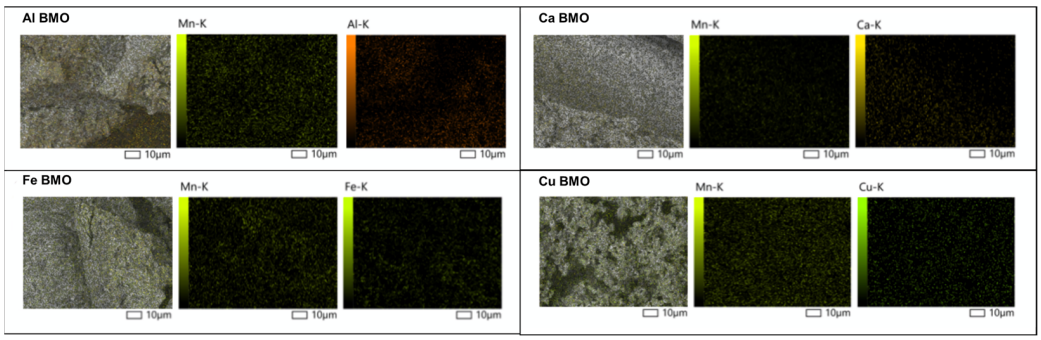
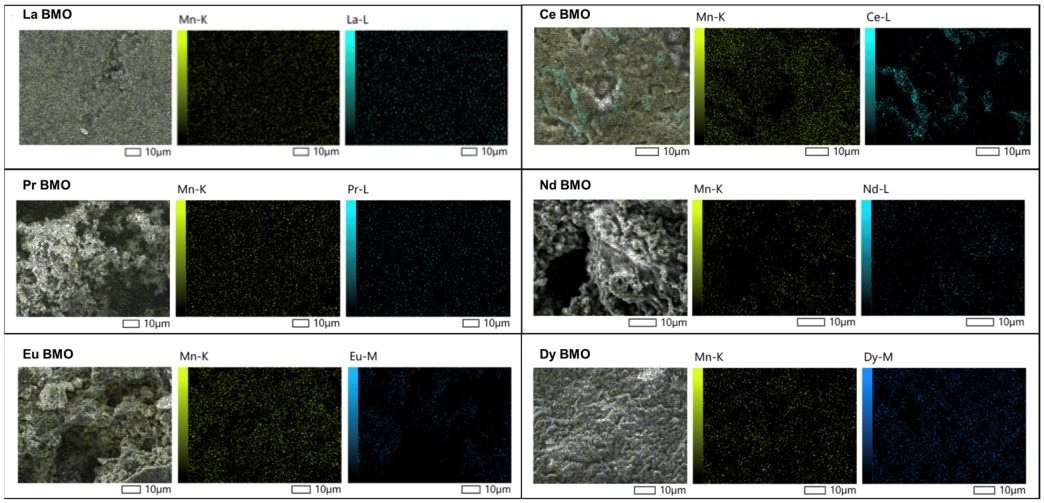


Figure 3. SEM images and EDX element maps of M BMO samples where M is a main group or transition metal.

(**A**)



(**B**)

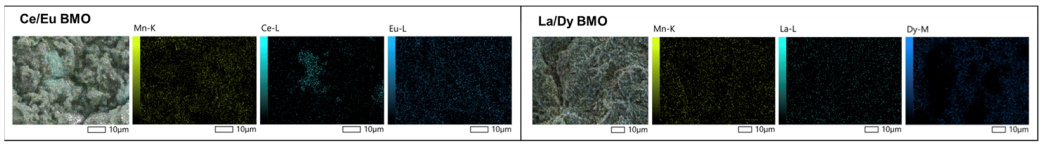


Figure 4. SEM images and EDX element maps of M BMO samples where M is a rare earth element (**A**), and M BMO where the sample was exposed to a 1:1 mixture of two rare earth elements (**B**).

The elemental compositions of the BMO materials following metal uptake screening experiments were quantified using ICP-OES and SEM/EDX to determine both the amount of manganese as well as the propensity for other metals to be incorporated. Elemental compositions for M BMO where M is a main group or transition metal are provided in Tables 1 and 2, and data for M BMO where M is a rare earth element are presented in Tables 3 and 4. BMO samples for ICP were prepared by dissolving ~10 mg of the solid in concentrated acid and diluting with water to a volume of 10 mL; further dilutions were performed, if needed. All samples were tested for the elements Mg, Al, K, Ca, Mn, Fe, and Cu. Any samples exposed to rare earth cations were also tested for La, Ce, Pr, Nd, Eu, and Dy. A summary of these results is shown in Table 1 for the main group/transition metal M BMOs and Table 3 for the rare earth M BMOs; additional ICP data are provided in Tables S1 and S2 in the Supplemental Materials. The results indicate that prior to the metal uptake studies, manganese makes up around 7% of the BMO material by mass and the alkali and alkaline metals magnesium, potassium, and calcium account for 2.76% of the mass. The remainder of the sample mass is expected to be composed of oxygen in the MnO_x and cellular material.

Table 1. Composition of M BMO materials, where M is a main group or transition metal, determined by ICP-OES. Samples were tested for magnesium, aluminum, potassium, calcium, manganese, iron, and copper. Reported mass percentages for an element are calculated based on the total mass of the sample.

Sample	Mass% Mn [1]	Mass% M	Mass% Mn + M	M:Mn Mole Ratio
BMO	7.08	N/A	7.08	N/A
Al BMO	9.78	1.36	11.14	0.283
Ca BMO	8.16	1.21	9.37	0.203
Fe BMO	9.71	5.20	14.91	0.175
Cu BMO	7.11	4.91	12.02	0.599

[1] In all samples, the amounts of metal detected other than Mn and the secondary metal, M, are minimal (each is <0.8% of the total mass with the exception of K in the BMO sample, which is 1.27%).

Table 2. Composition of M BMO, where M is a main group or transition metal, determined by SEM/EDX. For each sample, manganese, calcium, and potassium were measured as well as the M. Reported mass percentages for an element are calculated based on these metals that were measured.

Sample	Mass% Mn	Mass% M	Mass% Mn + M [1]	M:Mn Mole Ratio
BMO	75.36	---	75.36	---
Al BMO	81.41	17.14	98.55	0.429
Ca BMO	88.11	8.99	97.10	0.140
Fe BMO	63.63	33.73	97.36	0.521
Cu BMO	68.95	29.29	98.24	0.368

[1] The remainder of the measured mass is composed of Ca and K such that the total mass% sums to 100%.

Table 3. Composition of M BMO, where M is a rare earth metal or a combination of rare earth metals, determined by ICP-OES. Samples were tested for manganese and the rare earth elements lanthanum, cerium, praseodymium, neodymium, europium, and dysprosium. Reported mass percentages for an element are calculated based on the total mass of the sample.

Sample	Mass% Mn [1]	Mass% M	Mass% Mn + M	M:Mn Ratio
BMO	7.08	N/A	7.08	N/A
La BMO	8.62	3.92	12.54	0.180
Ce BMO	7.03	2.80	9.83	0.156
Pr BMO	9.75	3.18	12.93	0.127
Nd BMO	8.57	4.15	12.72	0.185
Eu BMO	12.56	4.83	17.83	0.139
Dy BMO	7.76	4.88	12.64	0.212
Ce/Eu BMO	8.63	1.67 (Ce) 2.88 (Eu) 4.55 (Ce + Eu)	13.18	0.076 (Ce:Mn) 0.121 (Eu:Mn) 0.189 (Ce + Eu:Mn)
La/Dy BMO	8.24	2.59 (La) 2.36 (Dy) 4.95 (La + Dy)	13.19	0.124 (La:Mn) 0.097 (Dy:Mn) 0.221 (La + Dy:Mn)

[1] In all samples, the amounts of other rare earth metals detected, other than M, are minimal (each is <0.2% of the total mass).

Table 4. Composition of M BMO, where the additional metal(s) M is a rare earth metal, determined by SEM/EDX. For each sample, manganese, calcium, and potassium were measured as well as the M. Reported mass percentages for an element are calculated based on these metals that were measured.

Sample	Mass% Mn	Mass% M	Mass% Mn and M [1]	M:Mn Mole Ratio
BMO	75.36	N/A	75.36	N/A
La BMO	64.60	29.38	93.98	0.180
Ce BMO	61.70	29.51	91.21	0.183
Pr BMO	68.13	26.63	94.76	0.152
Nd BMO	64.89	31.49	96.38	0.240
Eu BMO	80.99	13.84	94.83	0.062
Dy BMO	74.19	20.35	94.54	0.093
Ce/Eu BMO	65.99	15.66 (Ce)		0.093 (Ce)
		8.97 (Eu)		0.049 (Eu)
		24.63 (Ce + Eu)	90.62	
La/Dy BMO	67.59	17.39 (La)		0.102 (La)
		10.24 (Dy)		0.051 (Dy)
		27.63 (La + Dy)	95.22	

[1] The remainder of the measured mass is composed of Ca and K such that the total mass% sums to 100%.

Following metal uptake, the ICP data indicate that the main group/transition metal M BMOs contain 7.11–9.78% Mn by mass, and that aluminum, calcium, iron, and copper are all incorporated into the material. In all cases, the metal uptake studies result in an increase in the mass of total metal present (Mass% Mn + M ranging from 9.37–14.91%). The M:Mn mole ratios of the M BMO materials indicate that the added metal is present in a lesser amount than Mn, and copper is incorporated to the greatest extent of the metals tested (M:Mn mole ratio of 0.599 compared to 0.283, 0.203, and 0.175 for Al, Ca, and Fe, respectively). The ICP data for the rare earth metal M BMOs indicate that all of these metals are also incorporated into the samples during the metal uptake experiments and manganese is present in 7.03–12.56% by mass. The M:Mn mole ratios of the rare earth elements in the M BMO materials are similar across all metals tested (M:Mn mole ratios ranging from 0.127–0.212) indicating comparable affinities for the BMO. Additionally, the competition studies show both metals are incorporated into the material; the BMO exposed to a 1:1 solution of Ce/Eu yielded a sample with Ce:Mn mole ratio of 0.076, Eu:Mn mole ratio of 0.121, and (Ce + Eu):Mn mole ratio of 0.189. Likewise, the BMO exposed to a 1:1 solution of La/Dy produced material with a La:Mn mole ratio of 0.124, a Dy:Mn mole ratio of 0.097, and a (La + Dy):Mn mole ratio of 0.221.

The composition of the BMO and M BMO materials was also measured using SEM/EDX. These data are presented in Tables 2 and 4 for the main group/transition metal M BMOs and rare earth BMOs, respectively. These data are consistent with the ICP results in that all of the metals tested are incorporated into the BMO material during the uptake experiments. For the main group and transition metals, the range of M:Mn mole ratios is similar to the ICP results (0.140–0.521), but the top metal is iron instead of copper. The rare earth data from SEM/EDX is also similar, with all rare earth elements being incorporated to roughly the same extent. However, the M:Mn mole ratios for Eu and Dy are smaller for the EDX measurement compared to the ICP value.

Adsorption isotherms for a representative light REE (Nd^{3+}), heavy REE (Dy^{3+}), and transition metal (Cu^{2+}) were experimentally obtained from a series of batch adsorption studies performed on treated discharge water samples from a municipal wastewater treatment facility that were spiked with Nd^{3+}, Dy^{3+}, and Cu^{2+} and treated with different dosages

of BMO. The data (Figure 5) were fitted into the Langmuir and Freundlich empirical isotherm shown in Figure 6. Dy^{3+} and Nd^{3+} fit better with the Langmuir isotherm, obtaining a maximum adsorption capacity of 2.4 and 2.0 mg/g, respectively. REE adsorption onto BMO can be speculated to occur at a 1:1 REE to adsorption site ratio, where adsorption equilibrium is not influenced by the adsorption of other metals. On the other hand, Cu^{2+} adsorption onto BMO fits with the Freundlich isotherm, while the experimental data set did not converge with the Langmuir isotherm. This could be indicative that other metals from the wastewater adsorbed onto BMO, other than Cu^{2+}, influence Cu^{2+} adsorption. These potential adsorption phenomena of REEs and Cu^{2+} are constrained within the equilibrium concentration range of 0–15 mg/L and specific system condition described. Although an initial rationalization about the adsorption activities has been made, further investigations including kinetic and thermodynamics studies need to be conducted to produce concrete evidence that elucidates the adsorption mechanism of metals onto BMO.

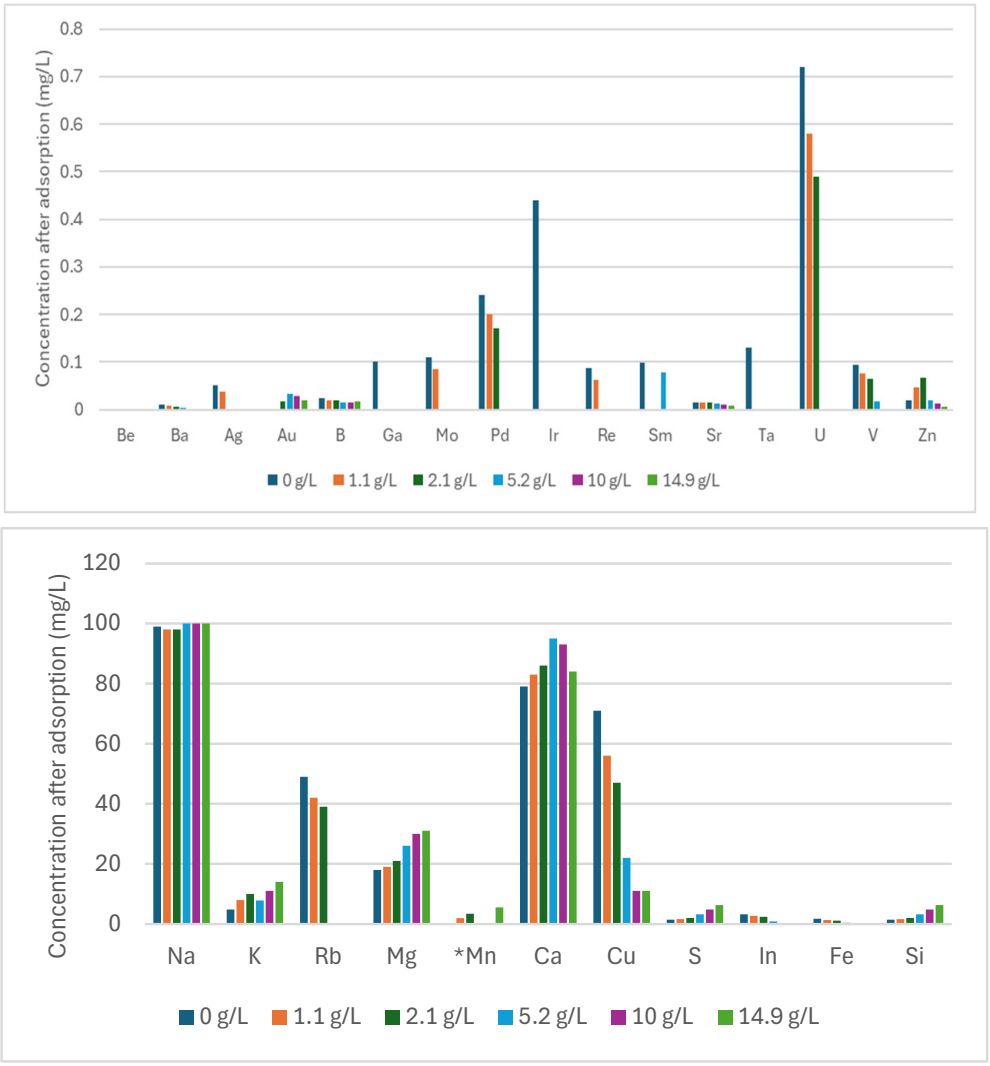


Figure 5. *Cont.*

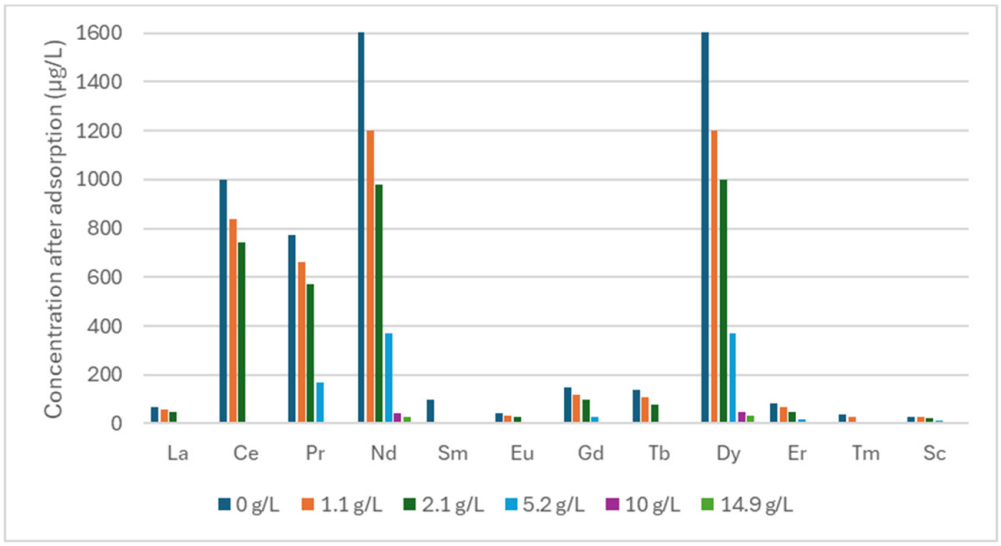


Figure 5. Comparison of different metals' concentrations in the wastewater effluent treated with BMO at different BMO dosages. The wastewater was dosed with 15 mg/L of Nd^{3+}, Dy^{3+}, and Cu^{2+} prior to the experiment. * The concentration of Mn in the wastewater after 5.2 g/L and 10 g/L BMO dosing were out of the instrument's detection limit.

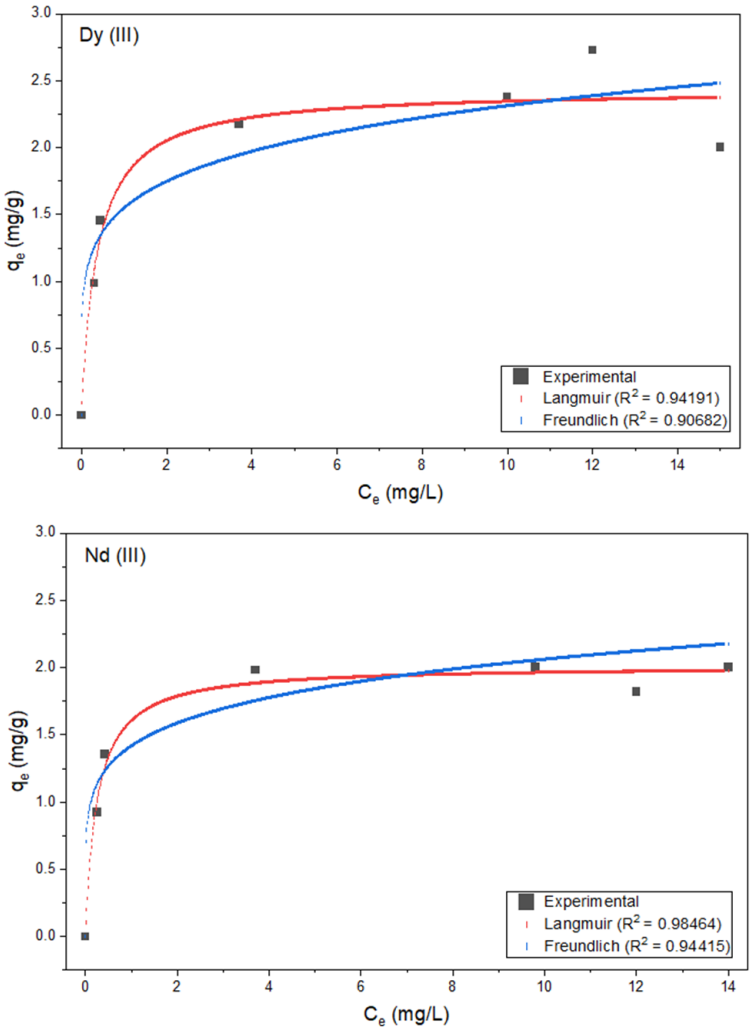


Figure 6. *Cont.*

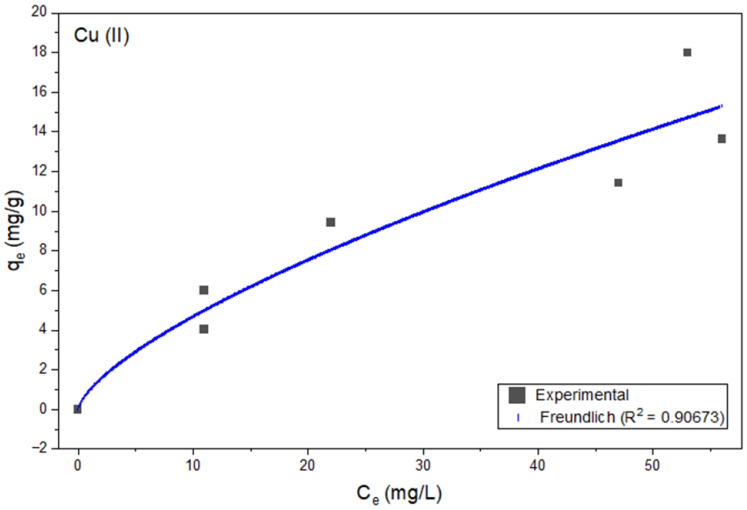


Figure 6. Adsorption isotherms for Dy^{3+}, Nd^{3+}, and Cu^{2+}. The experiments were replicated and collectively overlaid to produce the isotherms.

Characterization data for the M BMO materials indicate that all ten metals tested are incorporated into the BMO material. The resulting mixed metal materials may display properties that are altered or enhanced compared to the original BMO material. To further explore one case related to catalysis, the main group and transition metal BMO materials, Al BMO, Ca BMO, Cu BMO, and Fe BMO, were tested for their activity as water oxidation electrocatalysts. Catalyst inks for each M BMO material were deposited on glassy carbon electrodes, and linear sweep voltammetry (LSV) was performed in alkaline aqueous solutions with a pH of 13. The LSV voltammograms are shown in Figure 7; each electrode was scanned at a rate of 5 mV/s and each trace is the average of the results from three electrodes. The LSV data indicate that all catalyst inks show OER activity greater than the blank glassy carbon electrode, and that Al BMO, Ca BMO, and Cu BMO show activity similar to BMO. However, electrodes coated with the Fe BMO catalyst ink show higher water oxidation activity. For example, the current density for Fe BMO at a potential of 1000 mV vs. Ag/AgCl is more than double that of BMO (3.2 mA/cm^2 vs. 1.2 mA/cm^2 for Fe BMO and BMO, respectively, for an overpotential of η = 734 mV).

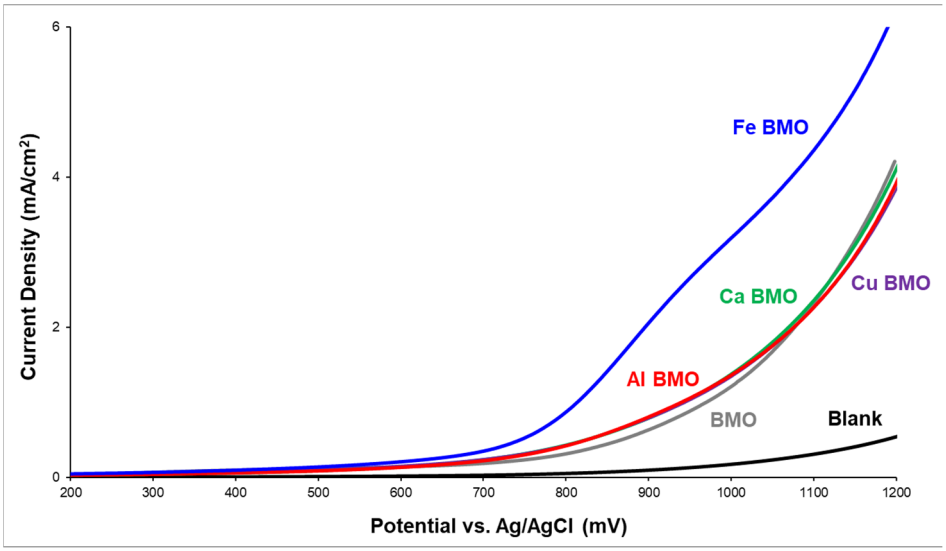


Figure 7. Linear sweep voltammograms for OER activity performed at a scan rate of 5 mV/s in 0.1 M NaOH solution using BMO and M BMO catalysts where M is a main group or transition metal.

4. Discussion

Biogenic manganese oxides are of interest for many applications that take advantage of their ability to adsorb or intercalate metal cations. These interactions play a key role in biogeochemical metal cycling [28], toxic metal remediation [15–17,29], and recovering critical and rare earth elements [14]. Biotic MnO_x produced by fungi or bacteria typically exhibit layered structures with poor crystallinity, and the presence of vacancies and/or Mn(III) sites promotes metal cation adsorption with a wide range of cation charges, sizes, and bonding geometries accommodated. Results from this present study are consistent with and expand upon these past results by demonstrating that BMO produced by *Pseudomonas putida* MnB1 readily adsorbs all ten of the metal cations investigated in the metal uptake screening studies. This encompasses main group metals: calcium and aluminum, transition metals: iron(III) and copper(II), and rare earth elements: lanthanum, cerium, praseodymium, neodymium, europium, and dysprosium. This is a wider range of metals than has typically been screened in a single study, and of particular interest are the REE results.

As the recovery and sequestration of critical metals becomes more important to meet global energy and environmental demands [30], the need to identify systems and materials to facilitate these processes will become more important. In fact, a recent report that highlighted the ability of biotic hydrous MnO_x to adsorb a wide range of metals focused on materials produced by the fungi *Paraphaeophaeria sporulosa* and *Stagnospora* sp. to recover rare earth elements as well as cobalt and yttrium from acid mine drainage [14]. The batch adsorption/isotherm studies performed in our work are proof-of-concept that the unfunctionalized BMO produced by *Pseudomonas putida* MnB1 using the current study's protocol has potential in REE sequestration from real water streams. Separation and concentration of REEs were not attempted, but in this study, the authors preliminarily demonstrated that the unfunctionalized BMO was able to adsorb REEs in a real water stream, as highlighted in Table 5. Sequestration of REEs using non-biogenic MnO_x typically involves precipitation [31]. Phosphorylated non-biogenic MnO_2 was reported to remove total rare earth elements (TREEs) of 7.1 mg/g from a synthetic acid mine drainage solution [32]. When phosphate groups are introduced into BMO, Wang et al. reported La(III) adsorption capacity of 538 mg/g extracted from a synthetic mixed metal solution [33]. The BMO described in this current work demonstrates adsorption activity for REEs in treated wastewater effluent despite the presence of other competitive adsorbing metals shown in Figure 5, in addition to residual nitrate and other anions typically present in the wastewater effluent that varies temporally. Strategies to enforce selectivity, improve concentration, and enhance purity of REEs from BMO are outside the scope of this screening study but can involve pretreatment of the wastewater to remove Group II and transition metals followed by leaching or incineration of BMO to liberate the REEs.

Table 5. Relevant literature for REE sequestration with MnO_x.

MnO_x Type	Max Adsorption Capacity (mg/g)	Aqueous Medium	Adsorption Conditions	Reference
Unfunctionalized biogenic manganese oxide (BMO)	Nd^{3+}: 2.01 Dy^{3+}: 2.43 Total REEs: 5.56	Real wastewater effluent spiked with 15 mg/L Dy^{3+}, Nd^{3+}, and Cu^{2+} with trace REE impurities from Dy^{3+}/Nd^{3+}, salt used for spiking	Contact time: 20 min Temperature: 25 °C Dosage: 2 g BMO/L pH of medium = 4.4 Conductivity of medium = 2.5 mS/cm	This study
Chemical δ-MnO_2	(Precipitation)	Synthetic seawater	Contact time: 3–130 h Temperature: 25 °C Dosage: 1 g δ-MnO_2 precipitate/g TREE pH of medium = 4.8–6.8	[31]

Table 5. *Cont.*

MnO_x Type	Max Adsorption Capacity (mg/g)	Aqueous Medium	Adsorption Conditions	Reference
PO_4-functionalized chemical MnO_2	Total REEs: 7.07	Synthetic acid mine drainage	Contact time: 20 h Dosage: 33 L $MnSO_4$(aq)/mg total REE-containing solution pH of medium = 2.21–2.36	[32]
PO_4-functionalized BMO	La^{3+}: 537.9	Synthetic mixed metal solution	Contact time: 45 h Temperature: 25 °C Dosage: 0.013 g P-BMO/L pH of medium = 4.0	[33]

Of note, the BMO material used in this study is composed of manganese oxide produced by *Pseudomonas putida* MnB1, as well as the bacterial cells from the organism. The manganese oxide material is produced on the surface of the cells and all attempts to remove the cellular material to isolate manganese oxide resulted in changes to the MnO_x structure. Therefore, this material was used without purification. While this provides a straightforward, convenient path to produce BMO, the presence of cellular material in the BMO material potentially complicates the interpretation of the metal cation uptake experiments due to the many possible interactions with organic and inorganic components. However, previous studies on bacterial biofilms indicate that the presence of organic matter does not impact the adsorption of trace zinc or lead cations onto MnO_x, and that the metals adsorbed preferentially to the manganese oxide [16,18]. Nonetheless, two other recent studies indicate that biomass may play an important role in and facilitate adsorption under some conditions [14,34]. Therefore, it appears that the identity and concentration of the metal, type of biomass, and pH of the system all contribute to the extent that the organic component contributes to the adsorption process. Our preliminary SEM/EDX results on MnB1 cells grown in the absence of manganese show that this material does adsorb iron when exposed to a 100 ppm Fe^{3+} solution (Figure S2 and Table S3) indicating that the role of the cellular material in our system should be investigated further.

In addition to our BMO material providing a promising pathway for metal sequestration and recovery, the resulting mixed metal BMO materials may also be useful in their own right, for example, as catalysts or electrocatalysts. Several MnO_x materials with additional metals incorporated into them have significant activity for different catalytic processes [35–39]. Our initial focus is on catalyzing the water oxidation half-reaction, which is a challenging component of water splitting [40]. Inspired by the oxygen-evolving complex in photosystem II [28,41–44], manganese oxide catalysts have been the focus of many OER studies [4,6,45], and more recently, biogenic manganese oxides have been targeted [3,5]. We previously demonstrated that the BMO material reported in this study showed promise for electrochemical water oxidation [5]. Since OER catalysts based on mixed metal oxides often outperform single metal oxide materials [44,46–48], the M BMOs produced in this study represent an easily accessible collection of materials that can be tested. The LSV data in Figure 7 show a catalytic wave corresponding to water oxidation for all of the M BMO materials tested. The Al BMO, Ca BMO, and Cu BMO materials are indistinguishable from BMO alone. However, Fe BMO electrodes show a lower potential for the onset of the catalytic wave and higher current densities. Based on this enhanced OER activity, the Fe BMO material will be the focus of future studies, and additional mixed metal BMO materials will be investigated.

5. Conclusions

In this study, biogenic manganese oxide material produced by *Pseudomonas putida* MnB1 was investigated for its ability to uptake metal upon exposure to a metal cation

solution. Ten metal cations, which included main group, transition, and rare earth metals, were tested, and all were readily incorporated into the BMO material. This indicates that this is a promising method for metal sequestration and a straightforward route to prepare mixed metal BMO materials. Several of the mixed metal BMO materials were tested electrochemically for their catalytic activity towards water oxidation, and the Fe BMO material demonstrated significantly higher current densities than the BMO material. Additionally, proof-of-concept batch adsorption studies were performed for a representative light REE (Nd^{3+}), heavy REE (Dy^{3+}), and transition metal (Cu^{2+}) using real wastewater effluent. The results indicated the REEs on BMO best fit a Langmuir isotherm while Cu^{2+} was better modeled by the Freundlich isotherm, and they suggest that the BMO material in this study is promising for sequestering REEs and other metals from real water streams.

Supplementary Materials: The following supporting information can be downloaded at https://www.mdpi.com/article/10.3390/oxygen6020013/s1: Figure S1: SEM images and EDX element maps of BMO samples; Table S1: Additional ICP-OES data for M BMO materials, where M is a main group or transition metal; Table S2: Additional ICP-OES data for M BMO materials, where M is a rare earth metal or a combination of rare earth metals; Figure S2: SEM images and EDX element maps of MnB1 cell material samples grown in the absence of manganese, and the same MnB1 material after exposure to a 100 ppm iron solution; Table S3: Composition of MnB1 cell material after exposure to a 100 ppm iron solution as determined by SEM/EDX; Figure S3: SEM images and EDX element maps of birnessite following exposure to a 100 ppm iron cation solution; Table S4: Composition of birnessite following exposure to a 100 ppm iron cation solution as determined by SEM/EDX.

Author Contributions: Conceptualization, K.L.S. and S.E.S.; methodology, J.R.A.R., K.L.S. and S.E.S.; formal analysis, E.M., J.R.A.R. and S.E.S.; investigation, E.M., G.D., C.J., A.B., N.P.-R., J.B., C.R., M.Y., L.S., J.R.A.R. and S.E.S.; resources, K.L.S. and S.E.S.; writing—original draft preparation, E.M., J.R.A.R., K.L.S. and S.E.S.; writing—review and editing, E.M., J.B., J.R.A.R., K.L.S. and S.E.S.; visualization, E.M., J.R.A.R., K.L.S. and S.E.S.; supervision, K.L.S. and S.E.S.; project administration, K.L.S. and S.E.S.; funding acquisition, K.L.S. and S.E.S. All authors have read and agreed to the published version of the manuscript.

Funding: The XRD facility at Southeast Missouri State University was supported by the National Science Foundation under Award Number 1919985.

Data Availability Statement: The raw data supporting the conclusions of this article will be made available by the authors on request.

Conflicts of Interest: The authors declare no conflicts of interest. The funders had no role in the design of the study; in the collection, analyses, or interpretation of data; in the writing of the manuscript; or in the decision to publish the results.

Abbreviations

The following abbreviations are used in this manuscript:

MnO_x	Manganese oxide
REE	Rare earth element
OER	Oxygen evolution reaction
BMO	Biogenic manganese oxides
XRD	X-ray diffraction
ICP-OES	Inductively coupled plasma optical emission spectroscopy
SEM/EDX	Scanning electron microscopy/energy-dispersive X-ray spectroscopy
TREE	Total rare earth elements
LSV	Linear sweep voltammetry

References

1. Guo, J.; Guo, H.; Liu, J.; Zhong, F.; Wu, Y. Manganese(II) Oxidizing Bacteria as Whole-Cell Catalyst for β-Keto Ester Oxidation. *Int. J. Mol. Sci.* **2020**, *21*, 1709. [CrossRef]
2. Stobbe, E.R.; de Boer, B.A.; Geus, J.W. The Reduction and Oxidation Behaviour of Manganese Oxides. *Catal. Today* **1999**, *47*, 161–167. [CrossRef]
3. Fu, W.; Hyler, F.P.; Sanchez, J.; Jaramillo, T.F.; Velázquez, J.M.; Tao, L.; Britt, R.D. Biogenic Manganese Oxide Synthesized by a Marine Bacterial Multicopper Oxidase MnxG Reveals Oxygen Evolution Activity. *ACS Catal.* **2024**, *14*, 7232–7242. [CrossRef]
4. Robinson, D.M.; Go, Y.B.; Mui, M.; Gardner, G.; Zhang, Z.; Mastrogiovanni, D.; Garfunkel, E.; Li, J.; Greenblatt, M.; Dismukes, G.C. Photochemical Water Oxidation by Crystalline Polymorphs of Manganese Oxides: Structural Requirements for Catalysis. *J. Am. Chem. Soc.* **2013**, *135*, 3494–3501. [CrossRef] [PubMed]
5. Morales, E.; Formanski, L.N.; Sarah, S.E.; Kari, S.L. Characterizing Biogenic Mnox Produced by *Pseudomonas putida* MnB1 and Its Catalytic Activity towards Water Oxidation. *Life* **2024**, *14*, 171. [CrossRef] [PubMed]
6. Pokhrel, R.; Goetz, M.K.; Shaner, S.E.; Wu, X.; Stahl, S.S. The "Best Catalyst" for Water Oxidation Depends on the Oxidation Method Employed: A Case Study of Manganese Oxides. *J. Am. Chem. Soc.* **2015**, *137*, 8384–8387. [CrossRef]
7. Meng, Y.; Song, W.; Huang, H.; Ren, Z.; Chen, S.-Y.; Suib, S.L. Structure–Property Relationship of Bifunctional MnO_2 Nanostructures: Highly Efficient, Ultra-Stable Electrochemical Water Oxidation and Oxygen Reduction Reaction Catalysts Identified in Alkaline Media. *J. Am. Chem. Soc.* **2014**, *136*, 11452–11464. [CrossRef]
8. Remucal, C.K.; Ginder-Vogel, M. A Critical Review of the Reactivity of Manganese Oxides with Organic Contaminants. *Environ. Sci. Process. Impacts* **2014**, *16*, 1247–1266. [CrossRef]
9. Forrez, I.; Carballa, M.; Verbeken, K.; Vanhaecke, L.; Schlüsener, M.; Ternes, T.; Boon, N.; Verstraete, W. Diclofenac Oxidation by Biogenic Manganese Oxides. *Environ. Sci. Technol.* **2010**, *44*, 3449–3454. [CrossRef]
10. Zhang, H.; Huang, C.-H. Oxidative Transformation of Triclosan and Chlorophene by Manganese Oxides. *Environ. Sci. Technol.* **2003**, *37*, 2421–2430. [CrossRef]
11. Tran, T.N.; Kim, D.-G.; Ko, S.-O. Synergistic Effects of Biogenic Manganese Oxide and Mn(II)-Oxidizing Bacterium *Pseudomonas putida* Strain MnB1 on the Degradation of 17 α-ethinylestradiol. *J. Hazard. Mater.* **2018**, *344*, 350–359. [CrossRef] [PubMed]
12. Zhu, C.; Li, H.; Wang, Y.; Ma, H.; Laipan, M.; Wang, M.; Xu, J. Characteristics and Applications of MnO_x and Its Modified Materials in Environmental Pollution Control: A Review. *J. Environ. Chem. Eng.* **2024**, *12*, 112384. [CrossRef]
13. Ghosh, S.K. Diversity in the Family of Manganese Oxides at the Nanoscale: From Fundamentals to Applications. *ACS Omega* **2020**, *5*, 25493–25504. [CrossRef]
14. Boothe-Lordon, T.J.; Capo, R.C.; Stewart, B.W.; Olds, T.A.; Rosenfeld, C.E. Critical Metal Adsorption by Biotic and Abiotic Hydrous Manganese Oxides: Implications for Acid Mine Drainage Resource Recovery. *ACS Omega* **2025**, *10*, 42577–42588. [CrossRef] [PubMed]
15. Yin, H.; Yan, X.; Zhu, C.; Kwon, K.D.; Gu, X.; Zhao, W.; Lanson, B.; Li, W.; Ma, J.; Li, Y.; et al. Cadmium Isotope Fractionation During Adsorption onto Edge Sites and Vacancies in Phyllomanganate. *Environ. Sci. Technol.* **2024**, *58*, 13498–13508. [CrossRef]
16. Nelson, Y.M.; Lion, L.W.; Shuler, M.L.; Ghiorse, W.C. Lead Binding to Metal Oxide and Organic Phases of Natural Aquatic Biofilms. *Limnol. Oceanogr.* **1999**, *44*, 1715–1729. [CrossRef]
17. Villalobos, M.; Bargar, J.; Sposito, G. Mechanisms of Pb(II) Sorption on a Biogenic Manganese Oxide. *Environ. Sci. Technol.* **2005**, *39*, 569–576. [CrossRef]
18. Wilson, A.R.; Lion, L.W.; Nelson, Y.M.; Shuler, M.L.; Ghiorse, W.C. The Effects of pH and Surface Composition on Pb Adsorption to Natural Freshwater Biofilms. *Environ. Sci. Technol.* **2001**, *35*, 3182–3189. [CrossRef]
19. Kim, D.-G.; Nhung, T.T.; Ko, S.-O. Enhanced Adsorption of Heavy Metals with Biogenic Manganese Oxide Immobilized on Zeolite. *KSCE J. Civ. Eng.* **2016**, *20*, 2189–2196. [CrossRef]
20. Chen, B.-R.; Sun, W.; Kitchaev, D.A.; Mangum, J.S.; Thampy, V.; Garten, L.M.; Ginley, D.S.; Gorman, B.P.; Stone, K.H.; Ceder, G.; et al. Understanding Crystallization Pathways Leading to Manganese Oxide Polymorph Formation. *Nat. Commun.* **2018**, *9*, 2553. [CrossRef]
21. Li, W.N.; Yuan, J.; Shen, X.F.; Gomez-Mower, S.; Xu, L.P.; Sithambaram, S.; Aindow, M.; Suib, S.L. Hydrothermal Synthesis of Structure- and Shape-Controlled Manganese Oxide Octahedral Molecular Sieve Nanomaterials. *Adv. Funct. Mater.* **2006**, *16*, 1247–1253. [CrossRef]
22. Cestaro, R.; Rheingans, B.; Schweizer, P.; Müller, A.; Vockenhuber, C.; Cancellieri, C.; Jeurgens, L.P.H.; Schmutz, P. Well-Defined Synthesis of Crystalline MnO, Mn_2O_3, and Mn_3O_4 Phases by Anodic Electrodeposition and Calcination. *J. Am. Ceram. Soc.* **2024**, *107*, 8676–8690. [CrossRef]
23. Spiro, T.G.; Bargar, J.R.; Sposito, G.; Tebo, B.M. Bacteriogenic Manganese Oxides. *Acc. Chem. Res.* **2010**, *43*, 2–9. [CrossRef] [PubMed]

24. Villalobos, M.; Toner, B.; Bargar, J.; Sposito, G. Characterization of the Manganese Oxide Produced by *Pseudomonas putida* Strain MnB1. *Geochim. Cosmochim. Acta* **2003**, *67*, 2649–2662. [CrossRef]
25. Romano, C.A.; Zhou, M.; Song, Y.; Wysocki, V.H.; Dohnalkova, A.C.; Kovarik, L.; Paša-Tolić, L.; Tebo, B.M. Biogenic manganese oxide nanoparticle formation by a multimeric multicopper oxidase Mnx. *Nat. Commun.* **2017**, *8*, 746. [CrossRef]
26. Tebo, B.M.; Bargar, J.R.; Clement, B.G.; Dick, G.J.; Murray, K.J.; Parker, D.; Verity, R.; Webb, S.M. Biogenic Manganese Oxides: Properties and Mechanisms of Formation. *Annu. Rev. Earth Planet. Sci.* **2004**, *32*, 287–328. [CrossRef]
27. Jiang, S.; Kim, D.G.; Kim, J.; Ko, S.O. Characterization of the Biogenic Manganese Oxides Produced by *Pseudomonas putida* Strain MnB1. *Environ. Eng. Res.* **2010**, *15*, 183–190. [CrossRef]
28. Hocking, R.K.; Brimblecombe, R.; Chang, L.-Y.; Singh, A.; Cheah, M.H.; Glover, C.; Casey, W.H.; Spiccia, L. Water-Oxidation Catalysis by Manganese in a Geochemical-Like Cycle. *Nat. Chem.* **2011**, *3*, 461–466. [CrossRef] [PubMed]
29. Stewart, B.D.; Bone, S.E.; Santelli, C.M. Transition Metal Recovery Using Manganese-Oxidizing Microbes and Recycled Carpet Fiber. *Environ. Sci. Technol.* **2025**, *59*, 19910–19920. [CrossRef] [PubMed]
30. United States Department of Energy. *DOE Critical Materials Assessment*; United States Department of Energy: Washington, DC, USA, 2023.
31. Ohta, A.; Kawabe, I. REE(III) Adsorption onto Mn Dioxide (δ-MnO_2) and Fe Oxyhydroxide: Ce(III) Oxidation by δ-MnO_2. *Geochim. Cosmochim. Acta* **2001**, *65*, 695–703. [CrossRef]
32. Depp, C.T.; Goodman, A.J.; Ranville, J.F. Enhanced REE Sorption to MnO_2 with PO_4 and P_2O_7 Ligands and Selective Desorption and Enrichment of Heavy REEs. *ACS Sustain. Resour. Manag.* **2025**, *2*, 2035–2043. [CrossRef]
33. Wang, Z.; Zhou, X.; Huang, Y.; Liu, J.; Wang, Y.; Zhang, Y.; Wang, X. A Novel Phosphate-Rich Biogenic Manganese Oxide for the Efficient Rare Earth Metal Ions Adsorption: Performance, Mechanism, and Applicability. *Ind. Eng. Chem. Res.* **2025**, *64*, 3486–3498. [CrossRef]
34. Peña, J.; Bargar, J.R.; Sposito, G. Role of Bacterial Biomass in the Sorption of Ni by Biomass-Birnessite Assemblages. *Environ. Sci. Technol.* **2011**, *45*, 7338–7344. [CrossRef] [PubMed]
35. Fan, Y.; Gao, H.; Song, Z.; Mao, Y.; Liu, W.; Chen, X.; Yu, H.; Zhang, X. Engineering Asymmetric Oxygen Vacancies in Binary Manganese Oxides: A Strategic Approach to Boost Catalytic Oxidation of Toluene. *J. Environ. Chem. Eng.* **2025**, *13*, 116480. [CrossRef]
36. Wu, S.; Yuan, C.; Huang, Z.; Xu, H.; Shen, W. Engineering Mn–O Strength in Manganese Oxide Catalyst to Enhance Propane Catalytic Oxidation. *Chem. Eng. J.* **2024**, *479*, 147928. [CrossRef]
37. Liao, Y.; Liu, P.; Zhang, J.; Wang, C.; Chen, L.; Yan, D.; Ren, Q.; Liang, X.; Fu, M.; Steven, L.S.; et al. Electrospun Ce–Mn Oxide as an Efficient Catalyst for Soot Combustion: Ce–Mn Synergy, Soot-Catalyst Contact, and Catalytic Oxidation Mechanism. *Chemosphere* **2023**, *334*, 138995. [CrossRef]
38. Sun, F.; Qin, J.; Cao, X.; Zhang, X.; Tang, X.; Wan, T.; Zhao, J.; Ma, J.; Long, Y. Cerium-Doped Manganese Oxide Catalyst for the Oxidative Coupling Synthesis of Fluorescent 2-Amino-1,9-Dimethyl-3*H*-Phenoxazin-3-One Using Atmospheric Oxygen. *ACS Sustain. Chem. Eng.* **2022**, *10*, 9087–9095. [CrossRef]
39. Panić, S.V.; Pantović Pavlović, M.R.; Varničić, M.M.; Tadić, V.; Stopić, S.; Friedrich, B.; Pavlović, M.M. Rare-Earth/Manganese Oxide-Based Composites Materials for Electrochemical Oxygen Reduction Reaction. *Catalysts* **2022**, *12*, 641. [CrossRef]
40. Lewis, N.S.; Nocera, D.G. Powering the Planet: Chemical Challenges in Solar Energy Utilization. *Proc. Natl. Acad. Sci. USA* **2006**, *103*, 15729–15735. [CrossRef] [PubMed]
41. Wiechen, M.; Najafpour, M.M.; Allakhverdiev, S.I.; Spiccia, L. Water Oxidation Catalysis by Manganese Oxides: Learning from Evolution. *Energy Environ. Sci.* **2014**, *7*, 2203–2212. [CrossRef]
42. Gates, C.; Ananyev, G.; Roy-Chowdhury, S.; Cullinane, B.; Miller, M.; Fromme, P.; Dismukes, G.C. Why Did Nature Choose Manganese over Cobalt to Make Oxygen Photosynthetically on the Earth? *J. Phys. Chem. B* **2022**, *126*, 3257–3268. [CrossRef]
43. Najafpour, M.M.; Zaharieva, I.; Zand, Z.; Maedeh Hosseini, S.; Kouzmanova, M.; Hołyńska, M.; Tranca, I.; Larkum, A.W.; Shen, J.-R.; Allakhverdiev, S.I. Water-Oxidizing Complex in Photosystem II: Its Structure and Relation to Manganese-Oxide Based Catalysts. *Coord. Chem. Rev.* **2020**, *409*, 213183. [CrossRef]
44. Najafpour, M.M.; Ehrenberg, T.; Wiechen, M.; Kurz, P. Calcium Manganese(III) Oxides ($CaMn_2O_4 \cdot x\,H_2O$) as Biomimetic Oxygen-Evolving Catalysts. *Angew. Chem. Int. Ed.* **2010**, *49*, 2233–2237. [CrossRef] [PubMed]
45. Huynh, M.; Bediako, D.K.; Nocera, D.G. A Functionally Stable Manganese Oxide Oxygen Evolution Catalyst in Acid. *J. Am. Chem. Soc.* **2014**, *136*, 6002–6010. [CrossRef] [PubMed]
46. Gerken, J.B.; Shaner, S.E.; Massé, R.C.; Porubsky, N.J.; Stahl, S.S. A Survey of Diverse Earth Abundant Oxygen Evolution Electrocatalysts Showing Enhanced Activity from Ni–Fe Oxides Containing a Third Metal. *Energy Environ. Sci.* **2014**, *7*, 2376–2382. [CrossRef]

47. McCrory, C.C.L.; Jung, S.; Ferrer, I.M.; Chatman, S.M.; Peters, J.C.; Jaramillo, T.F. Benchmarking Hydrogen Evolving Reaction and Oxygen Evolving Reaction Electrocatalysts for Solar Water Splitting Devices. *J. Am. Chem. Soc.* **2015**, *137*, 4347–4357. [CrossRef]
48. Forslund, R.P.; Hardin, W.G.; Rong, X.; Abakumov, A.M.; Filimonov, D.; Alexander, C.T.; Mefford, J.T.; Iyer, H.; Kolpak, A.M.; Johnston, K.P.; et al. Exceptional Electrocatalytic Oxygen Evolution via Tunable Charge Transfer Interactions in $La_{0.5}Sr_{1.5}Ni_{1-x}FexO_{4\pm\delta}$ Ruddlesden-Popper Oxides. *Nat. Commun.* **2018**, *9*, 3150. [CrossRef]

Disclaimer/Publisher's Note: The statements, opinions and data contained in all publications are solely those of the individual author(s) and contributor(s) and not of MDPI and/or the editor(s). MDPI and/or the editor(s) disclaim responsibility for any injury to people or property resulting from any ideas, methods, instructions or products referred to in the content.